Environmental Research Letters

LETTER • **OPEN ACCESS**

Are mercury emissions from satellite electric propulsion an environmental concern?*

To cite this article: Dan Fourie *et al* 2019 *Environ. Res. Lett.* **14** 124021

Environmental Research Letters

LETTER

Are mercury emissions from satellite electric propulsion an environmental concern?*

Dan Fourie[1], Ian M Hedgecock[2], Francesco De Simone[2], Elsie M Sunderland[3] and Nicola Pirrone[2]

[1] Independent researcher, Berkeley, California, United States of America
[2] CNR-Institute of Atmospheric Pollution Research, I-87036 Rende, Italy
[3] Harvard John A. Paulson School of Engineering and Applied Sciences, Harvard University, Cambridge, Massachusetts, United States of America

E-mail: nicola.pirrone@iia.cnr.it

Keywords: mercury pollution, satellite propulsion systems, new anthropogenic mercury source, ecosystems, atmospheric deposition

OPEN ACCESS

RECEIVED
29 April 2019

REVISED
6 October 2019

ACCEPTED FOR PUBLICATION
7 October 2019

PUBLISHED
27 November 2019

Abstract

A new generation of satellites for Earth observation and telecommunications are being designed and built with off the shelf components. This is driving down costs and permitting the launch of large satellite swarms with unprecedented spatial and temporal coverage. On-orbit maneuvers are commonly performed using ion thrusters. Mercury is one of the cheapest and easiest to store propellants for electric propulsion. While some mercury released in Low Earth Orbit may escape Earth's gravitational field, mercury emissions originating from many common orbital maneuvers will return to Earth. The environmental and human health implications of such releases have not been evaluated. Using an atmospheric chemical transport model, we simulate global deposition of mercury released from satellite propulsion systems. We estimate that 75% of the mercury falling back to Earth will be deposited in the world's oceans, with potentially negative implications for commercial fish and other marine life. Understanding the scale of this novel mercury source in a post-Minamata Convention world is necessary to limit ecosystem exposure to mercury contamination.

Nomenclature

X	value of the variable	
μ	mean	
σ	standard deviation	
v_x	exhaust velocity	m s^{-1}
v_o	satellite orbital velocity	m s^{-1}
v_i	ion velocity w.r.t. Earth	m s^{-1}
v_e	escape velocity	m s^{-1}
$v_\perp$	normal velocity	m s^{-1}
I_{sp}	specific impulse	s
g	standard gravity	m s^{-2}
G	gravitation constant	m^3 kg^{-1} s^{-2}
M	Earth mass	kg
r	radius from center of Earth	m
r_g	gyroradius	m
m	ion mass	kg
q	ion charge	C
B	magnetic field	T
ℓ	mean free path	m
n	number density	m^{-3}
σ	cross section	m^2
π	pi	
r_{He}	He atomic radius	m
r_{Hg}	Hg atomic radius	m

* The data that support the findings of this study are available from the corresponding author upon reasonable request.

Introduction

Environmental externalities of the booming space industry are being increasingly scrutinized. Risks from orbital debris are of serious concern (Liou and Johnson 2006) and mitigation plans are required for new satellite proposals (Federal Communications Commission 2017, 2018). More recently, the environmental impacts of combustion emissions from rocket engines are being examined (Ross and Vedda 2018). Plans for massive satellite constellations are expected

to increase the number of satellites in Low Earth Orbit (LEO, altitude <2000 km) by a factor of ten over the next 10–20 years (Ailor *et al* 2017, Le May *et al* 2018, Peterson *et al* 2018). For efficient orbit raising and orbital station-keeping (maneuvers required to maintain the desired altitude and path), many of these satellites will include electric propulsion systems, predominantly Hall thrusters (Lev *et al* 2017a, 2017b). Hall thrusters produce thrust by ionizing a propellant and accelerating it across an electric field (Gallimore 2008).

There has been little discussion of the risks associated with electric propulsion systems because the most common propellants, for example xenon, are not an environmental concern. However, the first ion thruster and the first orbital test in 1970 used the neurotoxicant, mercury, as a propellant because of its ease of storage, high molecular mass, and low ionization energy (Kaufman 1961, Kerslake and Ignaczak 1993). Concerns related to toxicity led to the abandonment of mercury as a propellant in the 1980s in favor of noble gases, predominantly xenon (Rawlin 1982). However, the high price of xenon ($2000/kg) coupled with burgeoning commercial space development has recently renewed interest in alternative, low-cost propellants such as mercury for electric propulsion (Kieckhafer and King 2007, Holste *et al* 2015, Saevets *et al* 2017, Elgin 2018).

The potential magnitude of mercury emissions from satellite electric propulsion depends on the propellant mass per satellite and the number of satellites. Satellites in the proposed constellations have masses in the range of 100–500 kg (Ailor *et al* 2017, Le May *et al* 2018), and propellant typically comprises a large fraction of the mass of satellites due to the large velocity changes required for orbital maneuvering (Gallimore 2008, Lev *et al* 2017b). As a representative magnitude, 2000 satellites (the average size of two approved constellations (Federal Communications Commission 2017, 2018)) each containing 100 kg of mercury propellant would emit 20 Mg of mercury per year over a 10 year lifetime. For comparison, this rate is about 50% of current annual total North American emissions, and about 1% of global annual anthropogenic mercury emissions (Muntean *et al* 2018, Streets *et al* 2019, UNEP 2019). These relatively large emissions from a single source will represent an even larger percentage under future emission scenarios, as more nations adhere to treaties such as the Minamata Convention on Mercury (UNEP 2017).

The Minamata Convention entered into force in August 2017 and has been ratified by 113 countries as of August 2019. The convention draws attention to anthropogenic mercury releases to the atmosphere, water, and soil and associated impacts on human health and ecosystems. The objective of the convention is to ban additional mining of mercury, and to phase-out mercury use in a number of manufacturing processes and everyday products. The convention aims to limit mercury emissions to the atmosphere and releases to terrestrial ecosystems from major anthropogenic sources such as fossil-fuel fired power plants, metals manufacturing facilities, caustic soda production plants, ore processing facilities including artisanal and small scale gold mines, waste incinerators, cement plants, and chemical production facilities. During the past two Conference of Parties in 2017 and 2018, the issues related to the interim storage of mercury and its disposal once it becomes waste, mercury contaminated sites, and human exposure were also addressed. In addition, among these anthropogenic sources, the potential contribution of mercury use as propellant in satellite propulsion has never been considered in past assessments of global mercury emissions and deposition (Pirrone *et al* 2010, UNEP 2013, 2017, 2019). However, the use of mercury as propellant in the aerospace sector is not specifically controlled by this convention. Therefore, just as rocket emissions are currently under scrutiny for their environmental impact (Ross and Vedda 2018), the potential repercussions of using mercury as a propellant in electric propulsion should be seriously considered.

In the 1970s, several studies were undertaken to examine environmental effects of cesium and mercury released from gridded ion thrusters as part of the Space Electric Rocket Test program (Lyon 1971). These studies were focused on implications for resultant ion belts (zones of energetic charged particles) rather than potential inputs of propellant to the troposphere. They found that mercury ions released at about 40–50 km s^{-1} at 1000 km altitude in a polar orbit are effectively constrained to spiraling back and forth between the polar magnetic mirror points (where charged particles trapped in the Earth's magnetic field reverse their direction). Roughly half of the ion trajectories have mirror points at altitudes below 100 km. These ions are rapidly removed from the magnetic field through neutralization and energy loss interactions with the atmosphere, potentially causing a faint artificial aurora. They are eventually removed by gravity into the lower atmosphere. The remaining trapped ions are most likely lost to space as they slowly form neutral atoms.

Simulations of xenon ion trajectories released at 44 km s^{-1} at altitudes from 15 000 to 115 000 km in near equatorial orbits suggest that roughly two-thirds of the ions under these conditions exit the magnetosphere and escape Earth's gravitation (Crofton and Hain 2007). About one-third were retained in a stable orbit over the 2–7 week simulation period. In a few cases, the ions reached the 30 km minimum altitude condition of the simulation, and therefore would be retained in the atmosphere. Ions released at lower altitudes were more likely to remain in stable orbits.

These studies serve as lower bounds on electric propulsion emissions retention, given that propellant from the proposed LEO mega constellations would be

released at a much slower initial velocity, and from a much lower orbit. The main objective of the present study is to characterize the potential environmental impact of widespread mercury use as a satellite propellant in LEO by tracing the fate of mercury ions from the satellite to Earth.

Methodology

We first briefly describe the orbital dynamics of the ions as they leave the satellite and are subsequently captured within the atmosphere. Subsequent subsections describe the chemical transport model used to simulate the deposition patterns to the Earth of mercury emitted from Hall thrusters.

Mercury emissions from Hall thrusters

For Hall thrusters in LEO, the velocity of the accelerated propellant ions (the exhaust velocity, v_x) is close to the satellite orbital velocity (v_o). This means that the initial propellant ejection direction with respect to the satellite orbital direction is significant, as it determines the initial kinetic energy of the ions with respect to Earth

$$v_x + v_o = v_i.$$

When performing orbit raising or drag make-up maneuvers (where the energy of the satellite needs to be increased), the thruster is fired in the opposite direction to the satellite trajectory in order to accelerate it. For a typical Hall thruster with a mean exhaust velocity of about 15 km s^{-1} (Gallimore 2008), the resultant mean ion velocity with respect to Earth (v_i) will be slower than the Earth escape velocity, up to an orbital altitude of about 4000 km (supporting calculations can be found in the appendix). Below this altitude, the vast majority of ions released during these types of maneuvers will be captured within the atmosphere, lacking the necessary energy to escape.

For propulsion maneuvers such as de-orbiting (where the thruster is fired in a retrograde direction in order to reduce the altitude of the satellite) the ions will have resultant speeds greater than Earth's escape velocity. Determining the fate of these ions is not as straightforward. The collisional mean free path (the mean distance that a particle will travel before encountering a collisional interaction with another particle) of mercury ions at about 1000 km altitude is 10^4–10^5 km (Johnson 1969), and their maximum gyroradius (radius of gyration of a charged particle in a magnetic field) is about 2 km (Thébault *et al* 2015), see appendix. This means that these ions will be trapped in a shell defined by the Earth's magnetic field lines with a thickness of the gyroradius, bouncing between the polar magnetic mirror points at most a few times before encountering an interaction with another particle. A few of the ions will be neutralized at a high altitude point in their path and will escape Earth's gravitational field. However, the ions are more likely to be neutralized in the lower, polar altitudes where the mean free path is shorter (<10 km at 200 km altitude) (Johnson 1969), and from where they will be less likely to escape before undergoing further decelerating interactions (Lyon 1971). Furthermore, ions ejected at small pitch angles to the magnetic field lines (e.g. along or against the direction of a satellite traveling in a near polar orbit, as most constellation satellites are planned) will have mirror points at low altitudes and therefore will most likely be decelerated and captured by the atmosphere rapidly (Lyon 1971). Despite these ions having resultant speeds greater than escape velocity, most will be retained in the atmosphere.

The decelerated mercury atoms may undergo continued re-ionization and re-neutralization as they traverse the ionosphere, but, as heavy particles, will gradually settle earthwards due to gravity (Brasseur and Solomon 2005) in a process similar to the atmospheric transport of meteoric ablation products (Feng *et al* 2013, Plane *et al* 2015). As atmospheric density increases and particle energies decrease at lower altitudes, most mercury will remain neutralized. Aside from this, the mercury chemistry in this region of the atmosphere is uncertain. The mercury will eventually diffuse to the turbopause (roughly 80–100 km altitude), which marks the boundary between the heterosphere and homosphere (Brasseur and Solomon 2005). To continue to trace the pathway of mercury from the turbopause to deposition on Earth, we turn to atmospheric modeling.

The global Hg chemistry and transport model

The ECHMERIT model was used to investigate the fate of mercury entering the atmosphere at high altitudes. ECHMERIT simulates the global chemistry and transport of mercury (Jung *et al* 2009, De Simone *et al* 2014), and is based on the Atmospheric General Circulation Model ECHAM5 (Roeckner *et al* 2003, 2006), developed at the Max Planck Institute for Meteorology (MPI-M, Hamburg, Germany). The model has been previously used for many applications, including the investigation of: (1) the role of different oxidation mechanisms on the global mercury cycle (De Simone *et al* 2014), (2) the impact of biomass burning on global mercury deposition (De Simone *et al* 2015, 2017a), (3) how current anthropogenic mercury emission inventories compare to each other (De Simone *et al* 2016), and (4) uncertainty in the global anthropogenic Hg emission source-receptor matrix (De Simone *et al* 2017b). The model uses a spectral grid, with a horizontal resolution ranging from T21 to T159. A horizontal resolution of T42 was selected for this study. Vertically, the standard model configuration is discretized with a hybrid-sigma pressure system with 19 or 31 non-equidistant levels up to 10 hPa (≈30 km). However, for this study, the model was extended to include a total of 39 non-equidistant levels in order to simulate the mesosphere up to 0.01 hPa (≈80 km), the approximate altitude to which

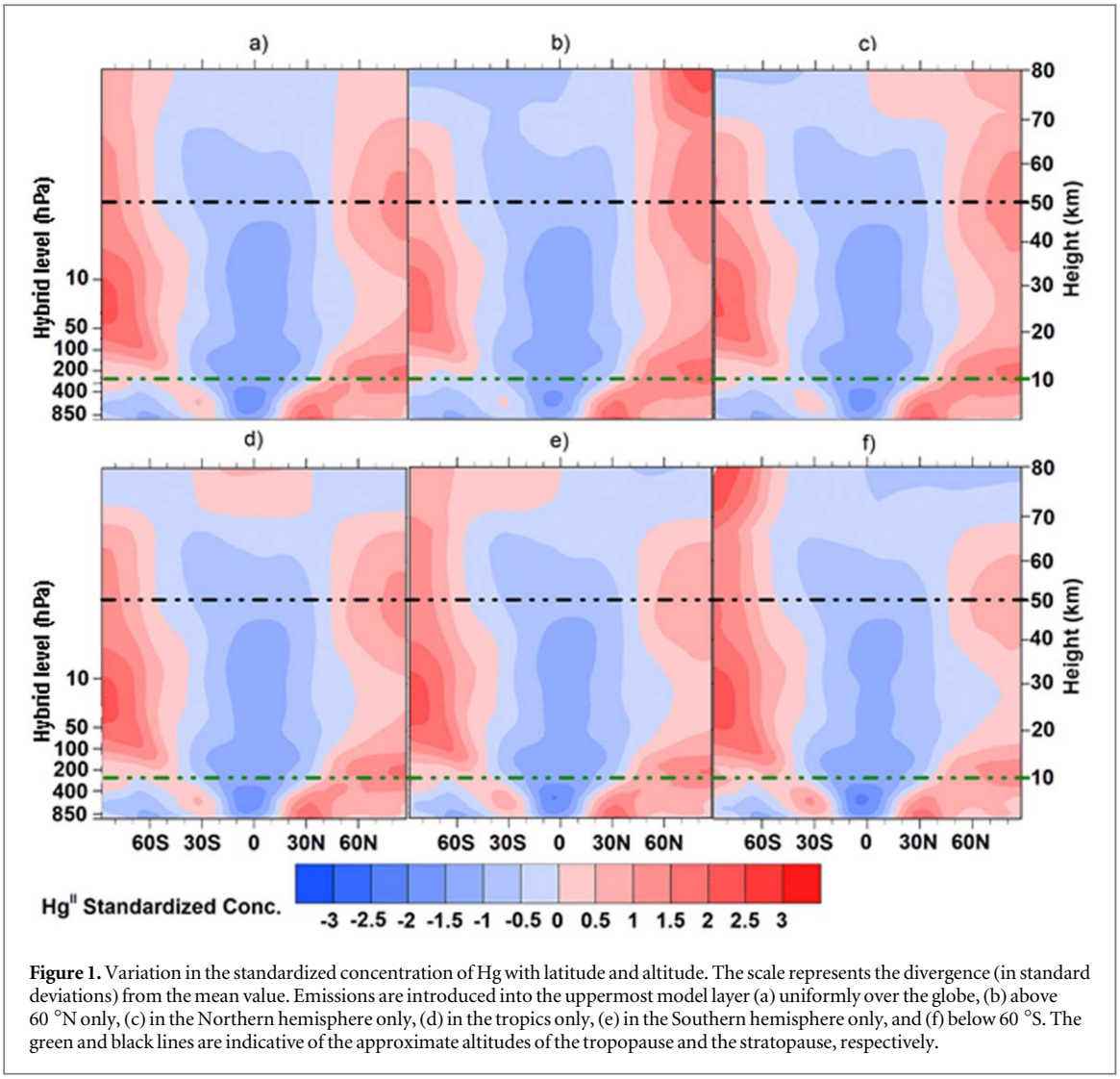

Figure 1. Variation in the standardized concentration of Hg with latitude and altitude. The scale represents the divergence (in standard deviations) from the mean value. Emissions are introduced into the uppermost model layer (a) uniformly over the globe, (b) above 60 °N only, (c) in the Northern hemisphere only, (d) in the tropics only, (e) in the Southern hemisphere only, and (f) below 60 °S. The green and black lines are indicative of the approximate altitudes of the tropopause and the stratopause, respectively.

the mercury will be transported due to gravitational settling.

For all simulations, an annual potential mercury emission rate from a constellation of satellites of 20 Mg yr^{-1} was used to force the model, as described above. More certainty on emission magnitudes would require more precise knowledge of planned constellation mission parameters such as orbital altitude, delta-v (the velocity change required for maneuvers), and lifetime, as well as simulation and statistical analysis of ion trajectories and interactions (as in Crofton and Hain 2007), which we recommend for a future study.

The simulations were initialized with real meteorological data (January 2001), and then run with standard forcing for a ten year spin up period. The subsequent five years of simulations were used to analyze the tropospheric concentration fields and terrestrial and marine deposition fluxes. In order to account for temporal uncertainty in the propellant emission rates, the results from these final five years of the simulations have been averaged to give annual values and then standardized ($[X - \mu]/\sigma$) to highlight the regions of high and low mercury concentrations, and to show more clearly the mercury transport patterns through the atmosphere.

In order to account for uncertainty in the spatial distribution and Hg speciation (oxidation state) of these emissions, an ensemble simulation approach was chosen (Parker 2013). A number of simulations were run, each with a different combination of spatial distribution and speciation flux input to the top of the model. The spatial distributions used were (a) globally uniform, (b) above 60 °N only, (c) Northern hemisphere only, (d) Tropics only, (e) Southern hemisphere only, and (f) below 60 °S only. The mercury speciation used was: (a) all elemental mercury (Hg^0), (b) all divalent mercury (Hg^{II}), or (c) all particulate mercury (Hg^P), for a total of eighteen simulations. The latter assumption (all Hg^P), although unlikely, was nonetheless considered for comparison purposes. To compensate for the relatively limited number of scenarios included in the ensemble, the bootstrap method (Mudelsee 2014), was used to calculate the average deposition fields that would be produced if a more comprehensive set of parameters and initial conditions had been tested (Parker 2013). To avoid

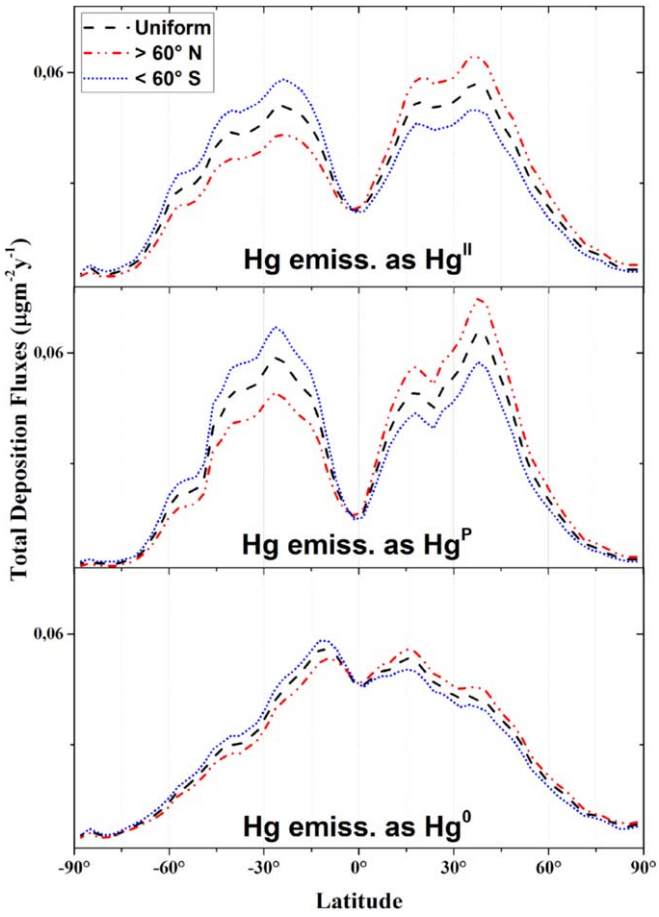

Figure 2. Latitudinal profiles of the total Hg deposition fluxes from nine of the simulations included in the ensemble. The cases where the emissions are constrained to just one hemisphere or to the tropics were omitted here for clarity because they proved to be very similar to the results from the simulation with uniformly distributed Hg emissions. Emissions were uniformly distributed (black line), constrained to above 60 °N (red line), below 60 °S (blue line), and as Hg^{II} (upper panel), Hg^{P} (central panel), and Hg^{0} (lower panel).

redundancy of information within the ensemble, a reduced or 'inspected' ensemble (Solazzo and Galmarini 2015) was identified to include only the results which differ the most (as in De Simone *et al* 2015, 2016, 2017a, 2017b). The similarity of the deposition fields was therefore assessed by means of both horizontal pattern correlation (Santer *et al* 1995, 1996) and the non-parametric Kolmogorov–Smirnov two-sample test, to include only those simulated Hg deposition fields where the test indicates that it is improbable (at a 95% level of confidence) that they belong to the same distribution.

Results and discussion

Model results show that convective mixing transports the Hg from the turbopause into the stratosphere, and eventually into the troposphere, consistent with our original hypothesis. The latitude-altitude profiles of atmospheric Hg concentration are similar irrespective of the location of the Hg emissions. All the simulations show that Hg predominantly descends into the stratosphere and troposphere at high latitudes, and that the highest concentrations at ground level occur at around 30 °N. Figure 1 shows the latitudinal profiles for six simulations in which the mercury from satellites enters the top of the model with different spatial distributions. In these cases, the mercury was introduced into the top model layer as Hg^{II}. Figure 1(a) shows the results for a uniform distribution of emissions, while figures 1(b)–(f) show the results when the emissions are confined to a single hemisphere, the tropics, or the poles. Higher concentrations outside of the emission region are predicted close to the stratopause and the tropopause over the North pole, and almost throughout the stratosphere over the South pole.

Figure 1 suggests that, wherever the Hg input occurs at the top of the model domain, the dominant atmospheric descent pathways are the polar vortices, which is consistent with middle atmosphere dynamics (Brasseur and Solomon 2005) and studies of meteorite ablation products (Feng *et al* 2013). These concentration visualizations illustrate the atmospheric transport patterns, but deposition fluxes describe the actual ecosystem inputs.

The deposition flux simulations, as illustrated by the profiles in figure 2, indicate generally similar patterns for the three different mercury species tested, with some variation due to differences in the

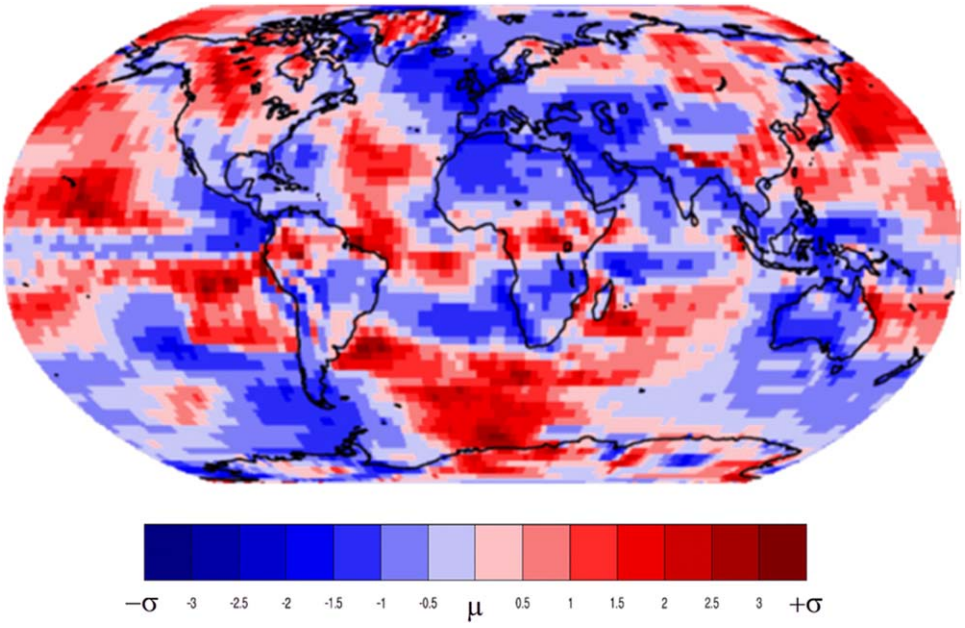

Figure 3. Geographical distribution of annual mercury deposition from satellite emissions (20 Mg yr^{-1}) shown as the probability density function obtained from the ensemble of simulations. Deposition is illustrated in terms of the average ($\mu = 0.03$ μgm^{-2} yr^{-1}) and standard deviation ($\sigma = 0.02$ μgm^{-2} yr^{-1}) of the ensemble.

depositional processes affecting each species. The high deposition flux from 22 °S to 22 °N° reflects the deep convective scavenging of Hg^{II} and Hg^{P} by precipitation and the higher concentrations in the troposphere at those latitudes (figure 1). As expected for a wet deposition process, the general deposition profiles for Hg^{II} and Hg^{P} are similar to the global rainfall distribution, except for the dip in the region of the equator. This dip is most likely due to most of the Hg^{II} and Hg^{P} emissions being scavenged before they can be transported to the equator. In contrast, the longer residence time of elemental mercury (Hg^{0}) allows for a much broader distribution of the deposition flux, with only a slight dip around the equator. Dry and wet deposition processes are less efficient at the poles than they are at mid-latitudes and in the tropics, hence the tailing off of the deposition flux above 75 °N and °S (Sprovieri *et al* 2016, Travnikov *et al* 2017).

The map in figure 3 highlights the geographical regions of highest and lowest potential impact from mercury contamination by satellite emissions. While the simulated deposition fields differ noticeably, it is evident from this ensemble deposition field that some regions are more likely to be impacted by mercury deposition from satellite emissions than others. Compared to deposition patterns from biomass burning (De Simone *et al* 2015) and terrestrial anthropogenic emissions (De Simone *et al* 2016), this distribution is more scattered globally as opposed to concentrated near centers of industry and population. This pattern is unsurprising considering the orbital origin of these emissions and the longer time spent in atmospheric transport. For this reason, may have outsized impact in regions not typically considered to have high deposition flux of mercury originating from satellite emissions.

At 20 Mg yr^{-1}, mercury emissions from satellites would represent about 1% of global anthropogenic mercury emissions. While this would already comprise a significant quantity from a single source (Pirrone *et al* 2010, Pacyna *et al* 2010), it could constitute an even larger fraction in future emissions scenarios as the signatories to the Minamata Convention continue to take steps to reduce their use of mercury and employ abatement measures. Table 1 compares total mercury deposition from this study's representative potential emissions rate with deposition resulting from anthropogenic emissions in 2010 (De Simone *et al* 2017b) as well as those from a Maximum Feasible Reduction (MFR) scenario in 2035 (Pacyna *et al* 2016). The table lists the average Hg deposition distribution among the different land regions and ocean basins from the simulation ensemble. Although released over a larger time window, mercury deposition resulting from these satellite emissions represents a large fraction of an entire year of terrestrial anthropogenic emissions in the MFR scenario.

Furthermore, about 75% of the mercury from satellite emissions is deposited in the oceans. This fraction is larger than the magnitude (63%) of land-based anthropogenic emissions that are eventually deposited to the oceans (De Simone *et al* 2017b). Marine fish are the predominant vector of methylmercury exposure to human populations in many countries (Sunderland 2007) and thus such deposition patterns could potentially affect future human exposure to mercury.

Table 1. Distribution of mercury deposition (Mg) by region resulting from satellite emissions of 20 Mg yr^{-1} compared to annual deposition rates (Mg yr^{-1}) for the MFR scenario and 2010 anthropogenic emissions, including confidence intervals. The geographical regions are based on those used in De Simone *et al* (2017b) and AMAP/UNEP (2013).

	Total deposition from a satellite emission rate of 20 Mg yr^{-1} over 10 years[a] Mg	Maximum Feasible Reduction scenario (2035)[b] Mg yr^{-1}	Anthropogenic emissions (2010)[c] Mg yr^{-1}
Total	200	281	1799
US and Canada	7.2 (6.6–7.9)	11.7	78.8 (67.2–88.4)
Central America	1.8 (1.6–1.9)	3.2	21.2 (18.2–23.8)
South America	5.9 (5.4–6.4)	9.4	58.3 (48.9–66.2)
Europe	1.6 (1.5–1.7)	4.8	36.5 (30.1–42.5)
North Africa	3.7 (3.2–4.1)	5.9	29.8 (35.5–42.4)
South Africa	7.0 (6.5–7.6)	12.0	78.7 (65.6–89.8)
Middle East	1.5 (1.3–1.7)	2.5	16.6 (14.5–18.2)
Russia and C. Asia	5.0 (4.7–5.4)	10.7	79.5 (69.3–89.3)
South Asia	2.2 (2.1–2.4)	7.9	36.3 (27.3–45.7)
East Asia	6.1 (5.5–7.0)	19.6	143 (115.2–178.5)
South East Asia	1.3 (1.0–1.5)	4.0	21.7 (18.3–24.5)
Australia	2.6 (2.5–2.8)	2.1	15 (12–17.7)
Arctic	2.2 (1.9–2.4)	4.8	36 (32.5–38.9)
Antarctica	0.9 (0.7–1.0)	2.3	5.5 (3.3–9.2)
North Atlantic	19.0 (17.9–20.1)		156 (140–165)
South Atlantic	18.0 (16.8–19.3)		101 (83–115)
North Pacific	45.3 (42.8–47.9)		437 (389–467)
South Pacific	39.6 (36.9–41.9)		251 (208–285)
Indian Ocean	24.3 (22.9–25.6)		176 (145–199)
Mediterranean Sea	0.9 (0.8–0.9)		9.2 (8–10.5)
Southern Ocean	1.9 (1.7–2.2)		11.5 (8.6–15.7)
Total Land	49.0 (44.3–53.9)	101.0	657 (558–775)
Total Oceans	148.8 (140.0–158.1)	180	1142 (982–1258)

[a] CI at the 95% level, bootstrap method from Mudelsee (2014).

[b] Pacyna *et al* (2016).

[c] Average from inventories used in De Simone *et al* (2017b).

For example, marine fish supply more than 85% of the methylmercury intake to the United States population and the largest contributing source region is the Pacific Ocean (Sunderland *et al* 2018). Both the tropical Pacific Ocean and Indian Ocean are important supply regions for global tuna fisheries, which account for the dominant fraction of methylmercury exposure for many individuals (Sunderland *et al* 2018). In figure 3, enhanced mercury deposition regions over the global oceans between 10° and 40° projected to result from satellite emissions correspond to some of the most important harvesting regions for global commercial fisheries (Zeller *et al* 2016).

Compounding this, mercury deposited to aquatic ecosystems atmospherically may be more readily converted to the bioacccumulative methylmercury species than legacy mercury that has resided in a watershed or strongly bound to organic carbon complexes for an extended period (Hintelmann *et al* 2002, Harris *et al* 2007). This means that newly deposited mercury from satellite propellant may have a proportionally larger impact on biotic accumulation than suggested by the increase in the magnitude of deposition alone. A recent study suggests that climate change will further enhance mercury bioaccumulation in fish in the future (Schartup *et al* 2019).

Conclusion

In this study, we have traced the fate of mercury released from satellites through the atmosphere to deposition at the Earth's surface. The relevant literature and our summary of the ion orbital dynamics indicate that the vast majority of mercury emissions from satellites in LEO with Hall thruster propulsion will reach the turbopause (about 80 km altitude). The results of our model simulations suggest that almost 75% of the mercury reaching the turbopause is deposited over the oceans, independent of the initial Hg release conditions considered. Mercury emissions from satellite constellations, if implemented at the scales proposed, would constitute a single addressable source representing about 1% of existing global anthropogenic mercury emissions. If launched, satellite electric propulsion using mercury propellant would be a major environmental concern. While beyond the scope of this work, even the possibility of a failure of a launch vehicle carrying a number of satellites would clearly represent a catastrophic risk to local ecosystems. The environmental impact of mercury propellant is not worth the satellite cost savings of moving away from existing non-toxic propellants. The use of mercury as a satellite propellant should be

monitored, quantified, and regulated by environmental intergovernmental organizations.

Acknowledgments

The authors are grateful to D M Murphy, P M Outridge, D A Jaffe, D J Jacob, S B Brooks, R P Mason, R Talbot, and C D Holmes for supporting discussions. We acknowledge the financial contribution from the European Commission—H2020, the ERA-PLANET programme (www.era-planet.eu) (Contract no. 689443) and IGOSP project (www.igosp.eu).

Appendix

A.1. Ion velocity calculation

The thruster exhaust ion velocity with respect to the Earth was calculated for the case where the ions leave the thruster in the direction opposite to the satellite velocity. The thruster exhaust velocity can be calculated from published values of specific impulse for typical Hall thrusters

$$v_x = gI_{sp}.$$

For a specific impulse (I_{sp}) of 1500 s, and standard gravity (g) of 9.8 m s^{-2}, v_x equals 14 700 m s^{-1}.

The satellite orbital velocity is dependent on orbital altitude

$$v_o = \sqrt{\frac{2GM}{r}}.$$

At 1200 km altitude, the distance from the center of the Earth (r) is 7578 km (6378 km + 1200 km). For Earth mass (M) of 6.0 × 10^{24} kg, gravitational constant (G) of 6.7 × 10^{-11} m^3 kg^{-1} s^{-2}, v_o equals 7255 m s^{-1}.

$$v_x + v_o = v_i.$$

Therefore, v_i equals 7445 m s^{-1}, which is less than the escape velocity (v_e) at 1200 km altitude.

$$v_e = \sqrt{\frac{2GM}{r}}.$$

At 1200 km altitude, v_e equals 10 260 m s^{-1}.

At 4000 km altitude, v_o equals 6200 m s^{-1}, so v_i equals 8500 m s^{-1}, which is less than v_e = 8800 m s^{-1}.

Below about 4000 km altitude, ions traveling at 15 km s^{-1} do not have sufficient energy to escape if ejected in the opposite direction to the satellite orbital direction.

A.2. Gyroradius calculation

The gyroradius of mercury ions in LEO was calculated using values for the strength of Earth's magnetic field provided by the International Geomagnetic Reference Field (Thébault *et al* 2015). The maximum gyroradius occurs at the highest velocity and smallest B-field

$$r_g = \frac{mv_\perp}{|q|\,B}.$$

The maximum velocity, normal to B-field, of an Hg ion released from a Hall thruster on a satellite in LEO is about 22 000 m s^{-1}. The approximate minimum strength of the Earth's magnetic field at 2000 km altitude (Thébault *et al* 2015) is 20 × 10^{-6} T. For the Hg molecular mass (m) of 3.3 × 10^{-25} kg, and the ion charge (q) of 1.6 × 10^{-19} C, the maximum gyroradius (r) of a mercury ion at 2000 km altitude is about 2 km.

A.3. Mean free path calculation

The mean free path of mercury ions in LEO was calculated using approximate values for atmospheric number density at that altitude (Johnson 1969).

The effective collision cross section between He (the dominant atmospheric species at these altitudes) and Hg is approximated from the atomic radii of the two species:

$$\sigma = \pi(r_{Hg} + r_{He})^2 = 2.5\,x\,10^{-19}\ \text{m}^2.$$

Mean free path is defined by:

$$\ell = \frac{1}{\sigma n}.$$

Altitude (km)	Number density[a] (m^{-3})	Mean free path (km)
200	1 * 10^{15}	4
1000	3.3 * 10^{11}	12 000
2000	3.3 * 10^{10}	120 000

[a] From Johnson (1969).

The collisional mean free path of mercury ions at 1000–2000 km altitude is 10^4–10^5 km.

ORCID iDs

Dan Fourie https://orcid.org/0000-0002-0348-8705
Elsie M Sunderland https://orcid.org/0000-0003-0386-9548

References

Ailor W, Peterson G, Womack J and Youngs M 2017 Effect of large constellations on lifetime of satellites in low earth orbits *J. Space Saf. Eng.* **4** 117–23

Brasseur G P and Solomon S 2005 *Aeronomy of the Middle Atmosphere: Chemistry and Physics of the Stratosphere and Mesosphere* (Netherlands: Springer)

Crofton M W and Hain T D 2007 Environmental considerations for xenon electric propulsion *30th Int. Electric Propulsion Conf. (Florence, Italy, 17–20 September, 2007)* (http://erps.spacegrant.org/uploads/images/images/iepc_articledownload_1988-2007/2007index/IEPC-2007-257.pdf)

De Simone F *et al* 2017a Particulate-phase mercury emissions from biomass burning and impact on resulting deposition: a modelling assessment *Atmos. Chem. Phys.* **17** 1881–99

De Simone F, Cinnirella S, Gencarelli C N, Yang X, Hedgecock I M and Pirrone N 2015 Model study of global

mercury deposition from biomass burning *Environ. Sci. Technol.* **49** 6712–21
De Simone F, Gencarelli C N, Hedgecock I M and Pirrone N 2014 Global atmospheric cycle of mercury: a model study on the impact of oxidation mechanisms *Environ. Sci. Pollut. Res.* **21** 4110–23
De Simone F, Gencarelli C N, Hedgecock I M and Pirrone N 2016 A modeling comparison of mercury deposition from current anthropogenic mercury emission inventories *Environ. Sci. Technol.* **50** 5154–62
De Simone F, Hedgecock I M, Carbone F, Cinnirella S, Sprovieri F and Pirrone N 2017b Estimating uncertainty in global mercury emission source and deposition receptor relationships *Atmosphere* **8** 236
Elgin B 2018 This silicon valley space startup could lace the atmosphere with mercury *Technical Report* Bloomberg Businessweek (https://bloomberg.com/news/articles/2018-11-19/this-space-startup-could-lace-the-atmosphere-with-toxic-mercury) (Accessed: 28 February 2019)
Federal Communications Commission 2017 Order and Declaratory Ruling, In the Matter of 'WorldVu Satellites Limited, Petition for a Declaratory Ruling Granting Access to the US Market for the OneWeb NGSO FSS System', IBFS File No. SAT-LOI-20160428-00041, FCC 17-77 (https://licensing.fcc.gov/myibfs/download.do?attachment_key=1247281)
Federal Communications Commission 2018 Memorandum Opinion, Order and Authorization, In the Matter of 'Space Exploration Holdings, LLC, Application For Approval for Orbital Deployment and Operating Authority for the SpaceX NGSO Satellite System', IBFS File No. SAT-LOA-20161115-00118, FCC 18-38 (https://licensing.fcc.gov/myibfs/download.do?attachment_key=1364689)
Feng W, Marsh D R, Chipperfield M P, Janches D, Höffner J, Yi F and Plane J M C 2013 A global atmospheric model of meteoric iron *J. Geophys. Res. Atmos.* **118** 9456–74
Gallimore A 2008 The physics of spacecraft hall-effect thrusters *61st Annual Meeting of the APS Division of Fluid Dynamics (San Antonio, TX, USA, 23–25 November, 2008)* (https://aps.org/units/dfd/meetings/upload/Gallimore_APSDFD08.pdf)
Harris R C *et al* 2007 Whole-ecosystem study shows rapid fish-mercury response to changes in mercury deposition *Proc. Natl Acad. Sci. USA* **104** 16586
Hintelmann H, Harris R, Heyes A, Hurley J P, Kelly C A, Krabbenhoft D P, Lindberg S, Rudd J W M, Scott K J and St. Louis V L 2002 Reactivity and mobility of new and old mercury deposition in a boreal forest ecosystem during the first year of the METAALICUS study *Environ. Sci. Technol.* **36** 5034–40
Holste K, Gärtner W, Köhler P, Dietz P, Konrad J, Schippers S, Klar P, Müller A and Schreiner P R 2015 In search of alternative propellants for ion thrusters *34th Int. Electric Propulsion Conf. (Hyogo-Kobe, Japan, 4–10 July, 2015)* (https://www.researchgate.net/publication/280157449)
Johnson C Y 1969 Ion and neutral composition of the ionosphere *Ann. IQSY* **5** 197–213
Jung G, Hedgecock I M and Pirrone N 2009 ECHMERIT v1.0—a new global fully coupled mercury-chemistry and transport model *Geosci. Model Dev.* **2** 175–95
Kaufman H R 1961 An ion rocket with an electron-bombarment ion source *Technical Report NASA-TN-D-585* National Aeronautics and Space Administration. Lewis Research Center, Cleveland, United States (https://www.osti.gov/biblio/4076793)
Kerslake W R and Ignaczak L R 1993 Development and flight history of the SERT II spacecraft *J. Spacecr. Rockets* **30** 258–90
Kieckhafer A and King L B 2007 Energetics of propellant options for high-power hall thrusters *J. Propul. Power* **23** 21–6
Le May S, Gehly S, Carter B A and Flegel S 2018 Space debris collision probability analysis for proposed global broadband constellations *Acta Astronaut.* **151** 445–55
Lev D R, Emsellem G D and Hallock A K 2017a The rise of the electric age for satellite propulsion *New Space* **5** 4–14
Lev D R *et al* 2017b The technological and commercial expansion of electric propulsion in the past 24 years *35th Int. Electric Propulsion Conf.* 8–12 October, 2017(USA: Georgia Institute of Technology) (https://researchgate.net/profile/Dan_Lev3/publication/326925975_The_Technological_and_Commercial_Expansion_of_Electric_Propulsion_in_the_Past_24_Years/links/5b707ad792851ca65056d434/The-Technological-and-Commercial-Expansion-of-Electric-Propulsion-in-the-Past-24-Years.pdf)
Liou J-C and Johnson N L 2006 Risks in space from orbiting debris *Science* **311** 340–1
Lyon W C 1971 A study of environmental effects caused by caesium from ion thrusters *Technical Report CR-122306* Goddard Space Flight Center, NASA (https://ntrs.nasa.gov/archive/nasa/casi.ntrs.nasa.gov/19720004693.pdf)
Mudelsee M 2014 *Climate Time Series Analysis: Classical Statistical and Bootstrap Methods* (Cham, Heidelberg, New York, Dordrecht, London: Springer)
Muntean M *et al* 2018 Evaluating EDGARv4.tox2 speciated mercury emissions ex-post scenarios and their impacts on modelled global and regional wet deposition patterns *Atmos. Environ.* **184** 56–68
Pacyna E G *et al* 2010 Global emission of mercury to the atmosphere from anthropogenic sources in 2005 and projections to 2020 *Atmos. Environ.* **44** 2487–99
Pacyna J M, Travnikov O, De Simone F, Hedgecock I M, Sundseth K, Pacyna E G, Steenhuisen F, Pirrone N, Munthe J and Kindbom K 2016 Current and future levels of mercury atmospheric pollution on a global scale *Atmos. Chem. Phys.* **16** 12495–511
Parker W S 2013 Ensemble modeling, uncertainty and robust predictions *Wiley Interdiscip. Rev. Clim. Change* **4** 213–23
Peterson G, Sorge M and Ailor W 2018 Space traffic management in the age of new space *Technical Report OTR 201800503* The Aerospace Corporation, Center for Space Policy and Strategy (https://aerospace.org/paper/space-traffic-management-age-new-space)
Pirrone N *et al* 2010 Global mercury emissions to the atmosphere from anthropogenic and natural sources *Atmos. Chem. Phys.* **10** 5951–64
Plane J M C, Feng W and Dawkins E C M 2015 The mesosphere and metals: chemistry and changes *Chem. Rev.* **115** 4497–541
Rawlin V 1982 Operation of the J-series Thruster using inert gas *16th Int. Electric Propulsion Conf. (New Orleans, Louisiana, 17–19 November, 1982)* (American Institute of Aeronautics and Astronautics) (https://doi.org/10.2514/6.1982-1929)
Roeckner E 2003 The atmospheric general circulation model ECHAM 5. PART I: model description *Technical Report* MPI-Report No. 349, 2003 Max Planck Institute for Meteorology (MPI-M), Hamburg, Germany
Roeckner E, Brokopf R, Esch M, Giorgetta M, Hagemann S, Kornblueh L, Manzini E, Schlese U and Schulzweida U 2006 Sensitivity of simulated climate to horizontal and vertical resolution in the ECHAM5 atmosphere model *J. Clim.* **19** 3771–91
Ross M and Vedda J A 2018 The policy and science of rocket emissions *Technical Report OTR2018-00493* The Aerospace Corporation (https://aerospace.org/sites/default/files/2018-05/RocketEmissions_0.pdf)
Saevets P A, Kim V P, Grdlichko D P and Smirnov P G 2017 Investigation of a low-power thruster on krypton propellant *Proc. Eng.* **185** 85–90
Santer B D, Taylor K E, Wigley T M L, Penner J E, Jones P D and Cubasch U 1995 Towards the detection and attribution of an anthropogenic effect on climate *Clim. Dyn.* **12** 77–100
Santer B D *et al* 1996 A search for human influences on the thermal structure of the atmosphere *Nature* **382** 39–46
Schartup A T, Thackray C P, Qureshi A, Dassuncao C, Gillespie K, Hanke A and Sunderland E M 2019 Climate change and overfishing increase neurotoxicant in marine predators *Nature* **572** 648–50
Solazzo E and Galmarini S 2015 A science-based use of ensembles of opportunities for assessment and scenario studies *Atmos. Chem. Phys.* **15** 2535–44

Sprovieri F *et al* 2016 Atmospheric Hg concentrations observed at ground-based monitoring sites globally distributed in the framework of the GMOS network *Atmos. Chem. Phys.* **16** 1–21

Streets D G, Horowitz H M, Lu Z, Levin L, Thackray C P and Sunderland E M 2019 Global and regional trends in mercury emissions and concentrations, 2010–2015 *Atmos. Environ.* **201** 417–27

Sunderland E M 2007 Mercury exposure from domestic and imported estuarine and marine fish in the US seafood market *Environ. Health Perspect.* **115** 235–42

Sunderland E M, Li M and Bullard K 2018 Decadal changes in the edible supply of seafood and methylmercury exposure in the United States *Environ. Health Perspect.* **126** 017006

Thébault E *et al* 2015 International geomagnetic reference field: the 12th generation *Earth, Planets Space* **67** 79

Travnikov O *et al* 2017 Multi-model study of mercury dispersion in the atmosphere: atmospheric processes and model validation *Atmos. Chem. Phys.* **17** 5271–95

UNEP 2013 Global mercury assessment 2013 *Technical Report* UN Environment Programme, Chemicals and Health Branch Geneva, Switzerland (https://unenvironment.org/explore-topics/chemicals-waste)

UNEP 2017 'MINAMATA CONVENTION ON MERCURY' (http://mercuryconvention.org)

UNEP 2019 Global mercury assessment 2018 *Technical Report* UN Environment Programme, Chemicals and Health Branch Geneva, Switzerland (https://unenvironment.org/explore-topics/chemicals-waste)

Zeller D *et al* 2016 Still catching attention: sea around us reconstructed global catch data, their spatial expression and public accessibility *Mar. Policy* **70** 145–52